ELSEVIER

Biophysical Chemistry 107 (2004) 229–241

Biophysical Chemistry

www.elsevier.com/locate/bpc

EXAFS studies of structural changes in fragile glasses of zinc nitrate and nickel nitrate hydrates

S. Ansell[a,*], G.W. Neilson[b]

[a]*ISIS Division, Rutherford Appleton Laboratory, Chilton, Didcot, Oxon OX11 0QX, UK*
[b]*H.H. Wills Physics Laboratory, University of Bristol, Tyndall Avenue, Bristol BS8 1TL, UK*

Received 16 September 2002; received in revised form 10 September 2003; accepted 16 September 2003

Abstract

The ionic structures of aqueous solutions of two sets of transition metal nitrates have been studied in the liquid and glass states by EXAFS spectroscopy. Experiments were carried out on $Zn(NO_3)_2 \cdot xH_2O$, with $x = 2$, 6, 12 and Ni(NO)·9HO over the temperature range $30 < T(K) < 250$. The glass transition regime was monitored by means of an in-situ DSC probe. The EXAFS data were analysed by recently developed Monte Carlo procedures, enabling a discussion of the glass structure in terms of pairwise and higher order correlations. Results for the zinc nitrate hydrates show complex behaviour depending on the concentration. This behaviour is explained in terms of first hydration shell stability and NO_3^- penetration. This result contrasts with that for the equivalent correlation in nickel nitrate, and is taken as evidence for a more extensive free energy landscape of zinc nitrate hydrates. The results are also consistent with the known hydration properties of Zn^{2+} and Ni^{2+}, and help explain why Zn^{2+} is biologically active in solution.

Keywords: EXAFS (Extended X-ray absorption fine structure spectroscopy); Glass transition; Zinc and nickel nitrates

1. Introduction

There are two aspects to this paper. The first is concerned with the fundamental physics of glass formation and how it relates to the structural dependence of local coordination around ions in fragile glasses. The results are therefore relevant to Kauzmann's ideas on the importance of entropic changes on glassification presented in his classic paper on the 'Nature of the Glassy State' [1]. The second is concerned with the chemistry of fragile glass formation and ionic denaturation of biological systems that contain complex ions, water molecules, and protein molecules. For example, it is becoming clear from our neutron diffraction isotopic substitution (NDIS) studies that the effectiveness of an ion to denature biological material is substantially governed by the degree to which it coordinates water molecules. It would appear that relatively weakly hydrated ions with waters of hydration in fast exchange [2–4] are more influential in the destabilisation of proteins due to the fact that they can interact directly with the

*Corresponding author.
E-mail address: s.ansell@rl.ac.uk (S. Ansell).

0301-4622/04/$ - see front matter © 2003 Elsevier B.V. All rights reserved.
doi:10.1016/j.bpc.2003.09.015

hydrophobic protein surface. The results below help explain why Zn^{2+} plays a crucial role in many biological processes.

The physics of fragile glasses is governed by their free-energy landscapes, which are more extensive than those of strong glass formers [3]. Strong glass formers such as SiO_2 are typically network-forming liquids and show very little variation of short and medium range order [5]. By contrast, fragile glasses such as aqueous electrolyte solutions which are much more difficult to form, have micro-structural changes in several thermodynamic regions of interest [6]. The first region is the fluid phase, where there is only one free energy minimum, which determines all the micro-structural properties. As the system is cooled without crystallisation below the freezing temperature (T_f) there is a region with an exponentially increasing number of free energy minima that the system progressively samples until the temperature reaches the dynamical transition point, T_D [7]. At T_D the system becomes trapped into one meta-stable state, and the local coordination around each ion can be considered trapped into a large set of microstates. This dynamical freezing causes non-equilibrium property such as the viscosity to diverge until the system reaches the Kauzmann temperature, T_K [8]. Without the intervention of the glass transition, the entropy of the supercooled liquid would paradoxically decrease below that of the crystal. The glass transition temperature, T_g, is not fixed, but is dependent on the cooling rate; it is expected that after an infinitely slow cooling process a glass would be formed at T_K. Above T_g, the cooling process is well understood in terms of mode coupling theory (MCT) [9]. Of current interest is the development of models that are applicable below T_g. These free-energy landscape models have enabled predictions to be on the annealing process [10]. In order to explore this regime we have carried out EXAFS studies of the local structure of the Zn^{2+} ion in three concentrated aqueous solutions of zinc nitrate.

From a chemical viewpoint, ions are believed to play a critical role in glass formation. For example, there is a wide range of glass forming ability amongst fragile glasses of aqueous electrolyte solutions, with those that contain complex ions (NO_3^-, SO_4^{2-} etc.) being easier to prepare [11]. Since Angell and Sare (1970) [6], published their classic paper on the glass transition temperature (T_g) of aqueous electrolyte solutions, it has been widely recognised that not only do many aqueous electrolyte solutions have glass-forming composition regions, but also their T_g values are closely related to their microscopic structures. Many attempts have been made to investigate the hydration structures of ions in aqueous ionic glasses in order to identify a unique structural signature associated with the glass. One of the more interesting suggestions to emerge from these investigations has been that proposed by Kivelson and coworkers [12], who hypothesized that if one is 'to seek structural indicators of the liquid–glass transition, one should look at functions that are not limited to two-body (pairwise) correlations'. The three foremost methods to determine interatomic structure in an aqueous electrolyte system have been critically reviewed [13]. It is well known that structural probes such as X-ray diffraction and neutron diffraction with isotopic substitution (NDIS) give information only on the pairwise structure of a liquid, however, EXAFS (Extended X-ray absorption fine structure spectroscopy) is sensitive to pair and higher order correlations. Moreover, EXAFS probes structure over a much short length scale. The EXAFS signal ($\chi(k)$) is composed of contributions from the radial distribution functions surrounding the photoabsorbing atoms. The pair correlation dominates far from the edge energy (E_0) but near E_0 the contribution is a combination of pair and higher order correlations which are mainly triplet terms.

In this paper, we apply the EXAFS technique to three $Zn(NO_3)_2{\cdot}xH_2O$ ($x=2$, 6, 12) glasses and to a reference glass system $Ni(NO_3)_2{\cdot}9H_2O$. All of the glasses were quenched in liq-N_2 and then slowly heated to observe the onset of structural relaxation. The EXAFS probe has several advantages for this type of work: (i) it is extremely sensitive to changes in the local environment of transition metal ions, (ii) it is fast, and data for a large numbers of state points can be obtained and rapidly monitored, (iii) an EXAFS experiment requires only an incoming and outgoing beam in a straight line; it is therefore possible to exploit

fully the large sample environment available without compromising the experimental measurement. (This last feature allowed us to monitor the system with a differential scanning calorimeter (DSC) system during the course of the experiment and ensure that the sample had not crystallised before or during the experiment) (iv) EXAFS also has the distinct advantage over diffraction techniques in that, as a spectroscopic probe, it is sensitive to can dynamical disorder of the molecular structure, and gives information on the interaction between the photoabsorbing atom and its nearest neighbours. It is this particular property that we exploit when discussing the annealing of the glass as it is heated to T_f.

In order to assess the general usefulness of our results we also note that the EXAFS method has a few disadvantages. The EXAFS probe has a $1/r^2$ signal decay which means that information outside of the first neighbour region is extremely poor quality [14]. Multiple scattering effects (triple and higher order correlations) make the determination of a unique structural solution difficult. Additional problems also arise because the value for E_0 (the effective-Fermi level) is not known to be better than 5 eV, and becomes a fitting parameter. Despite these obvious difficulties, we feel that the results in this paper which have been obtained by combining EXAFS data with a new Reverse Monte Carlo (RMC) procedure are robust and significant.

Previous EXAFS studies on Zn^{2+}, solutions have encountered problems in the interpretation of the structural results. Kuzmin et al. [15] assign low k features in the EXAFS spectrum to multiple scattering and indicative of a O–Zn–O bond angle of 124° in dilute solution. By contrast Munoz-Paez et al. [16] infer that the low k spectrum arises from the second coordination shell, a result in agreement with that obtained from X-ray diffraction [17]. However, both studies omit to include in the analysis the presence of hydrogen atoms which have been shown to be important when considering liquids [18]. In the present investigation we include the hydrogen atoms and limit the multiple scattering to that which gives rise to the most disordered signal. Although this criterion may lead to lower resolution in real space (e.g. causing broadening of the pair distribution functions of the photoabsorbing ion), the numerical consistency of this type of analysis means that we can make direct comparisons between glass in different thermodynamic states without bias.

2. Experimental

2.1. Sample preparation

Several nominally 3 M aqueous solutions of $Ni(NO_3)_2$ and $Zn(NO_3)_2$ were prepared by adding the dry salt (>99.9% pure) to an excess of deionised water. These solutions were then microfiltered through 0.1 μm filters and transferred into several pre-weighted glass tubes. These tubes were then slowly dried in an oven at 85 °C. The samples to be used for making glasses were selected from those that had not crystallised, and the water content was determined from the final bottle weight. Each of the four samples (three of zinc nitrate and one of nickel nitrate) used here was placed into an EXAFS cell using a thin glass capillary on a syringe. This procedure was used to reduce the possibility of crystallisation of the more concentrated samples. A 1.0 M solution of $Ni(NO_3)_2$ was also prepared and used as a reference system.

2.2. EXAFS experimental measurement

The experiments were carried out on BM29 at the ESRF. The beamline was used in its standard transmission mode. A monochromatic beam with energy resolution of approximately 0.25 eV at the Zn absorption edge (9.659 keV) (significantly better resolution than the Zn lifetime broadening of 1.67eV) was provided by two 311 Si crystals on the fixed exit monochromator [19]. Although the Si 111 configuration would have been preferable, this was precluded by the instrument user schedule. The absorption spectra were monitored by two Ar+He filled ion chambers with the proportions set to absorb 30% (pre-sample) and 70% (post-sample) of the beam. Two different sample environments were used. For the glass

samples the standard BM29 displex cryostat was used; this allowed temperatures down to 30 K to be achieved for flat plate samples. Liquid samples were placed between two Kapton sheets, which were then bolted together with a 50–200 μm PTFE spacer chosen to optimise the statistics of the EXAFS measurement at 30 K.

In order to make a glass, the filled EXAFS cell was attached to the cryostat candlestick and then plunged into liquid N_2 before being rapidly transferred into the pre-cooled cryostat. Since the crystalline forms of the solutions are often opaque, samples were checked for optical transparency whilst in the liquid N_2. This technique was used for all measurements below 100 K. Above this temperature, a Linkam optical DSC was used in which the windows had been replaced with Kapton, and the sample placed in an hermetically sealed aluminum sample can into which a PTFE washer had been placed. The washer was cut to the desired sample thickness, typically 150 μm. The lid of the DSC pan was compressed onto the PTFE spacer and the can was sealed. The DSC was taken to its lowest temperature (80 K) and the sample quenched in an open liquid nitrogen dewar. The sample was then dropped into the pre-cooled DSC, and resealed in approximately 10 s. The DSC was then mounted on the beamline to allow the X-ray beam to pass through the Kapton windows, and the slot cut in the silver DSC cell body. In this way DSC measurements could be taken in-situ at each temperature. The DSC trace was then used to ensure a glass transition was observed during the heating of the sample. If this was not observed, then it was assumed that the sample had crystallised during the loading process and the measurements were discarded.

In summary, the method of measurement was to quench the sample and then heat the sample in stages in the DSC. The heating was stopped at several temperatures and an EXAFS spectrum was acquired. EXAFS and DSC measurements were made simultaneously on three zinc nitrate aqueous glasses, $Zn(NO_3)_2{\cdot}2H_2O$ (I), $Zn(NO_3)_2{\cdot}6H_2O$ (II), $Zn(NO_3)_2{\cdot}12H_2O$ (III), and a nickel nitrate aqueous glass $Ni(NO_3)_2{\cdot}9H_2O$, (Figs. 1, 2a, 3a, 4a, 5a).

2.3. Data analysis method

The analysis of EXAFS spectra is usually carried out using several procedures involving a number of different analytical programs (Feff, GNXAS, Excurve [20–23]). Most of these codes have been designed for the analysis of crystalline data sets. When data sets from liquids are analysed in terms of crystalline models, problems arise due to the presence of large Debye–Waller and other Cumulant expansion factors being required. As a result, such modelling does not properly reproduce the disordered nature of a liquid. However, this procedure can lead to a close fit to the experimental data, but there are a large number of coupled variables and extreme care must be taken with the interpretation of the results when doing spectra to spectra comparisons. The Cumulant expansion is not a process that can be readily automated, which means it is difficult to use for direct comparisons between data sets. In recent years the GNXAS package has been improved to allow the refinement of the set of $g_{XY}(r)$s, where Y is any atom within the system and X is the photoabsorbing atom. In the work presented here, we have tried to refine this analysis. In order to include all the information available from the EXAFS experiment, we have simulated a box of $N=10\,000$ atoms following the standard Reverse Monte Carlo (RMC) routes [24]. In contrast to the diffraction based RMC we calculate both the pair ($g_{XY}(r)$) and triplet correlations $g_{XYZ}(r_1, r_2, \phi)$ at each step of the simulation and use the GNXAS code to calculate the signal weight for these correlation functions. A mesh of 0.02 Å is used for the pair correlation terms whilst for the triplet correlation term the mesh is 0.1 Å with 18 angular bins. This triplet mesh corresponds to a total of $\approx$7200 non-zero points per Y, Z atom type. This procedure takes into account all pair correlation terms from 0 to 7 Å and all triplet correlation terms from 0 to 4 Å, which involve a photoabsorbing atom.

At each step an atom is selected at random, its position changed and the tabulated $g_{XY}(r)$s and $g_{XYZ}(r_1, r_2, \phi)$s are updated and the theoretical $\chi(k)$ is calculated using

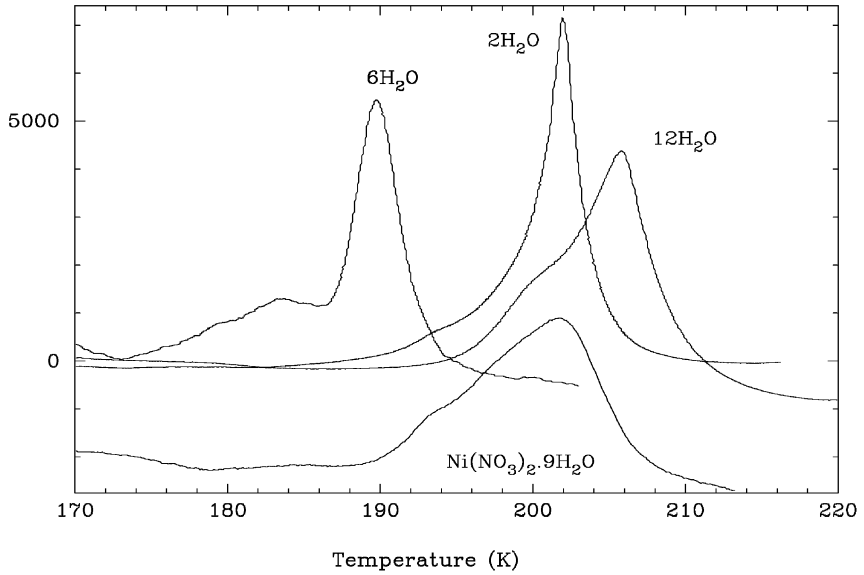

Fig. 1. Differential scanning calorimetry curves for $Zn(NO_3)_2 \cdot 2H_2O$; $Zn(NO_3)_2 \cdot 6H_2O$, $Zn(NO_3)_2 \cdot 12H_2O$ and $Ni(NO_3)_2 \cdot 12H_2O$. (displaced by 2000).

$$\chi_{\mathrm{comp}}(k) = \sum_{\mathrm{Y}}^{\mathrm{Species}} \rho \int_0^{\infty} 4\pi r^2 \gamma_{\mathrm{XY}}(k,r) g_{\mathrm{X,Y}}(r)\mathrm{d}r + \sum_{\mathrm{Y}}^{\mathrm{Species}} \sum_{\mathrm{Z}}^{\mathrm{Species}} \rho^2 \int_0^{\infty}\int_0^{\infty}\int_0^{\pi} 8\pi^2 r_1^2 r_2^2 \times \sin(\phi)\ \gamma_{\mathrm{XYZ}}(r_1,r_2,\phi,k) g_{\mathrm{XYZ}}(r_1,r_2,\phi)\mathrm{d}r_1\mathrm{d}r_2\mathrm{d}\phi \quad (1)$$

where

$$k = \sqrt{2m_e(E-E_0)}/\hbar,$$

$\gamma_{\mathrm{XY}}(r,k)$ is the EXAFS backscattering factor from atom Y at distance r from photoabsorbing atom X, and $\gamma_{\mathrm{XYZ}}(r_1, r_2, \phi, k)$ is the backscattering factor from the group with atom Y at distance r_1 and atom Z at distance r_2 from the photoabsorbing atom X. The angle ϕ is the made angle between atom Y the photoabsorbing atom X, and atom Y. The GNXAS routines calculate $\gamma_{\mathrm{XY}}(r,k)$ and $\gamma_{\mathrm{XYZ}}(r_1,r_2,\phi,k)$ for all the multiple scattering paths for the two atom or three atom cluster. The pair distribution of the sums are taken over all atom species in the simulation.

The first term of Eq. (1) is the single scattering or pairwise term and contributes approximately 90% of the total $\chi(k)$. The second term in Eq. (1) is due to triplet scattering and contributes mainly to the region approximately below $k=4.0$ Å^{-1}. The fourth and higher order terms contribute less than 1% to the signal and are therefore not included in the equation or the analysis.

The computed $\chi_{\mathrm{comp}}(k)$ is then compared with the experimental measurement and if the overall Chi-squared has decreased, the move is accepted, otherwise the move is accepted with an exponentially decreasing probability relative to the increase in Chi-squared.

The experimental χ_{expt} are extracted from the actual measurements $(\mu(E))$ using

$$\chi_{\mathrm{expt}}(k) = \frac{\mu(E) - \mu_0(E)}{\mu_0(E_0)} \quad (2)$$

with the routine from autobk [20].

In comparisons between computer $\chi_{\mathrm{comp}}(k)$ and experimental data $\chi_{\mathrm{expt}}(k)$, it is necessary to deal with the inaccuracy in the determination of E_0 from the experimental data. We do this by introducing a ΔE term which represents the variance of E_0 from that obtained by autobk (point of maximum slope in $\mu(E)$). Occasionally, when

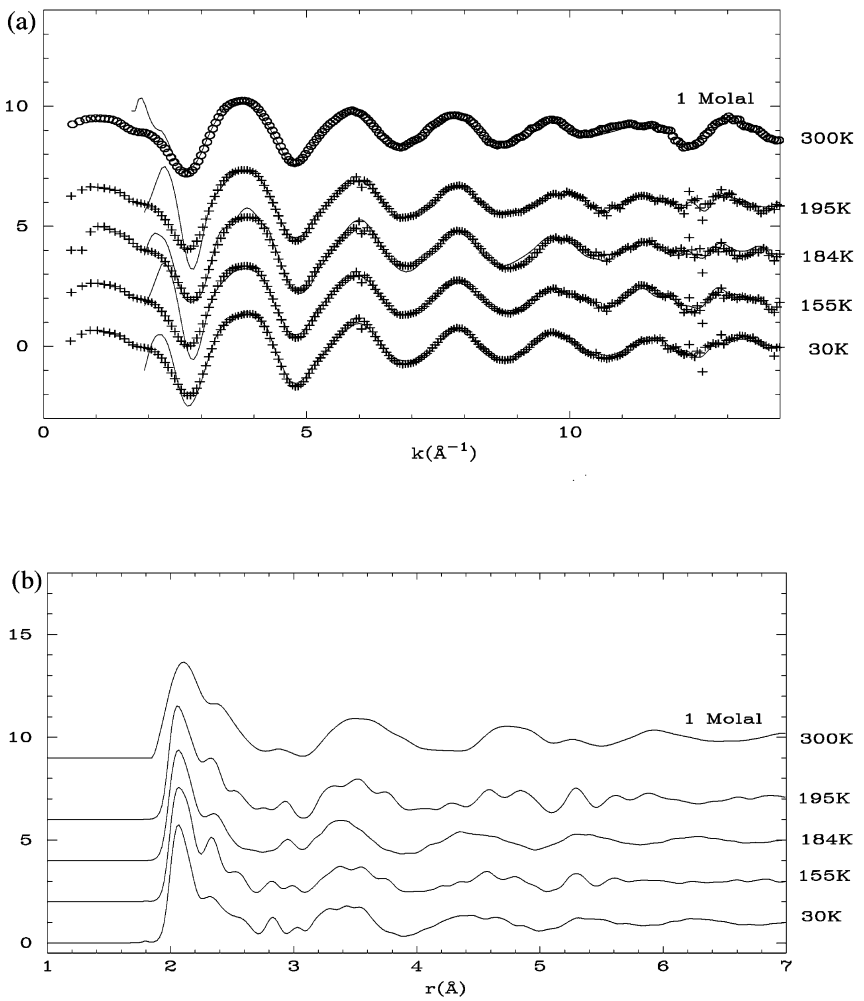

Fig. 2. (a) $\chi_{expt}(k)$ and $\chi_{comp}(k)$ for $Ni(NO_3)_2 \cdot 9H_2O$ as a function of temperature and 1 molal $Ni(NO_3)_2$ solution at 300 K. Note $T_g = 200$ K. (b) The corresponding $g_{NiO}(r)$s as calculated from the RMC simulation from Fig 2a.

selecting atoms to move in the simulation, ΔE is changed by a small amount. However, if the normal RMC acceptance criteria were applied, this move would almost always be rejected because it effectively re-scales the k range of the simulation and the Chi-squared fit would have increased. This can be partly overcome by recording the configuration of the RMC simulation prior to the ΔE change, then moving all the atoms within the simulation until the rate of acceptance for moves matches or is lower than that prior to the ΔE change. At this point the simulation decides whether to accept the ΔE move. If it accepts, the simulation is continued from this point and if it does not the simulation goes back to the recorded configuration.

This approach has the difficulty that for a multi-component system, where EXAFS data is unobtainable from all the constituent atoms, a degenerate solution set exists. This is the so-called 'inverse problem' since it has been proven [25] that it is always possible to find sets of different pair distribution functions that fits the EXAFS data. However, if additional information is availa-

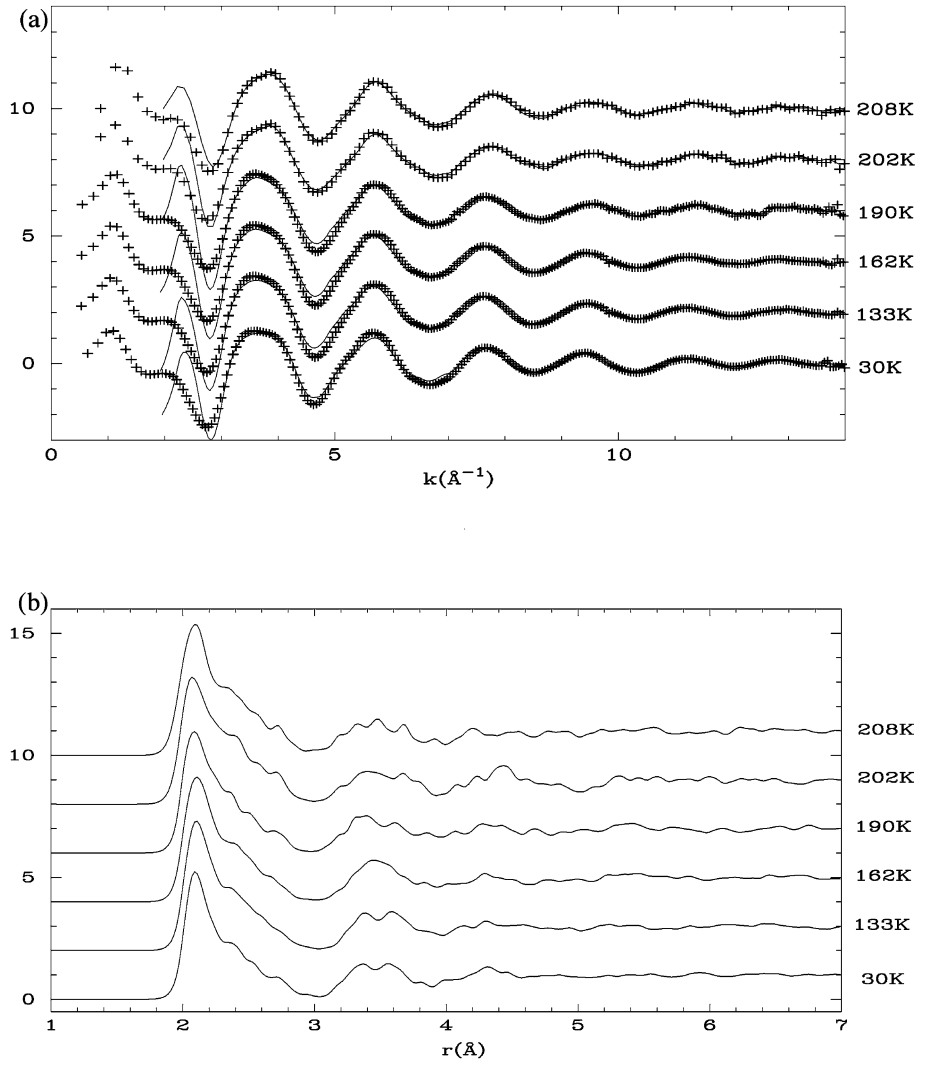

Fig. 3. (a) $\chi_{expt}(k)$ and $\chi_{comp}(k)$ for $Zn(NO_3)_2 \cdot 9H_2O$ as a function of temperature and 1 molal $Ni(NO_3)_2$ solution at 300 K. Note $T_g = 200$ K (b) The corresponding $g_{ZnO}(r)$s as calculated from the RMC simulation from Fig 3a.

ble or can be assumed, a stable approximate solution can be obtained. This is the approach used here, and the following constraints were implemented: (a) Hard spheres were assumed with radii equal to 0.75 times the actual ionic radii, (b) The metal ions (Ni or Zn) were assumed to have oxygen atoms in the closest shell; this was achieved by artificially adding a chi-squared modification component for those hydrogen atoms found within 2.3 Å of the metal ions. (c) The second moment of the $g(r)$s were multiplied by a smoothing factor and added into the Chi-squared to help drive the simulation towards a minimum signal solution. This term effectively drives the simulation towards more triple correlations and smoother $g(r)$, although these must still be consistent with the EXAFS signal and packing constrains. The parameter could not be increased indefinitely as there seems to be a maximum after which it dramatically decreased the fit to the

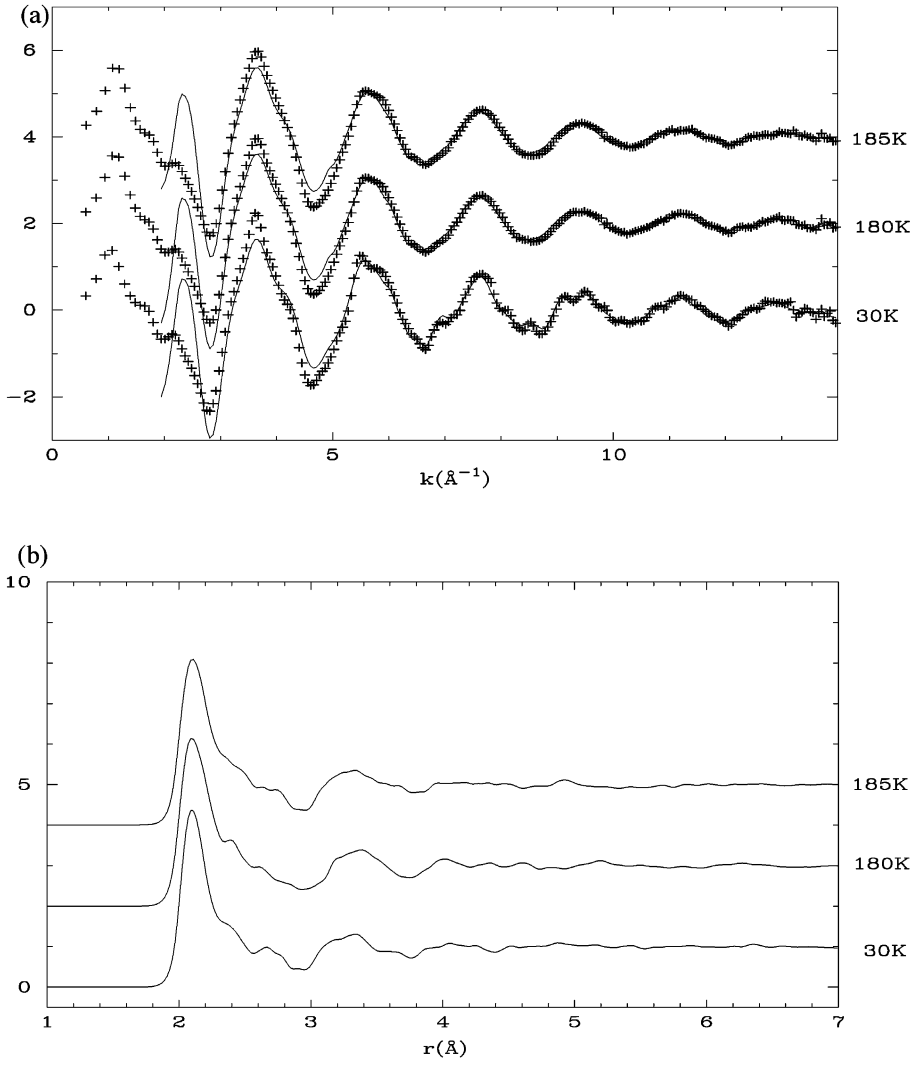

Fig. 4. (a) $\chi_{expt}(k)$ and $\chi_{comp}(k)$ for $Zn(NO_3)_2 \cdot 6H_2O$ as a function of temperature. Note $T_g = 190$ K. (b) The corresponding $g_{ZnO}(r)$s as calculated from the RMC simulation from Fig 4a.

EXAFS spectra. The smoothing parameter was set to a single fixed value well below its lowest distortion threshold value for all the analysis presented here. (d) The modification of E_0 with the ΔE_0 term is difficult to achieve within the simulation. This leads to possible ambiguity of distances within the results. Thus, in order to maintain consistent analysis between spectrums of the same chemical composition, ΔE_0 was initially fitted for each spectrum of a chemical composition, and then the simulations were re-started with a fixed ΔE_0 which was set to the mean ΔE_0 obtained from the group of spectra. This has the effect of increasing the absolute error of the position but decreasing the relative error between the different spectra.

This method has the advantage over using the Cumulant expansion methods since the fit considers all types of pair distribution functions.

The errors on the data are particularly important in this study since we observed small differences.

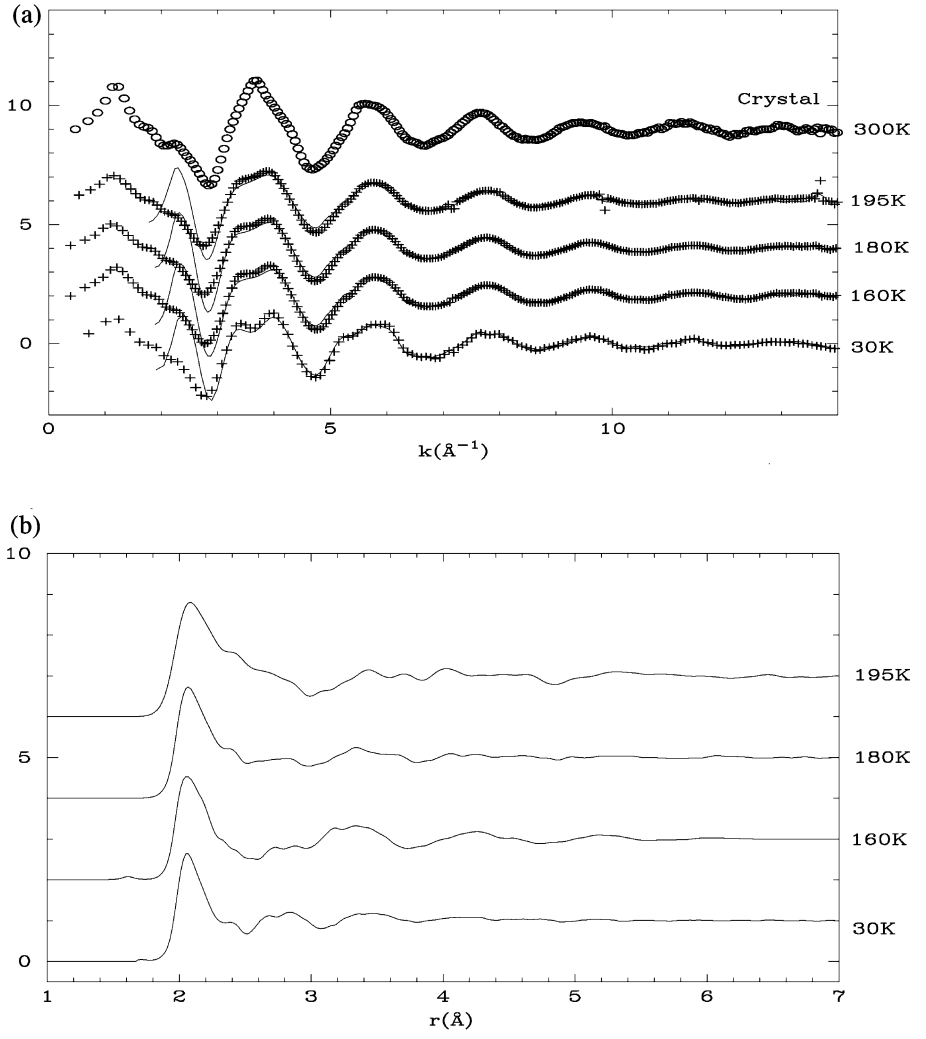

Fig. 5. (a) $\chi_{expt}(k)$ and $\chi_{comp}(k)$ for $Zn(NO_3)_2 \cdot 12H_2O$ as a function of temperature. Note $T_g = 208$ K. (b) The corresponding $g_{ZnO}(r)$s as calculated from the RMC simulation form Fig 5a.

In EXAFS analysis, the absolute error is primarily from the errors in E_0, the amplitude factors, and the backscattering phase angle. The RMC process used a fixed amplitude, phase angle and E_0 for all the runs of the same chemical composition, this reduces the error of reported differences between results from different spectra of the same chemical composition, at the expense of reducing the absolute accuracy of the measurement.

When we have fitted the measured $\chi_{expt}(k)$ with the RMC simulation, we obtain the radial distribution function $g_{ZnO}(r)$ and $g_{NiO}(r)$ for the zinc and nickel cations from the simulation, (Figs. 2b, 3b, 4b, 5b).

3. Results and discussion

The results for our standard nickel nitrate aqueous sample ($Ni(NO_3)_2 \cdot 9H_2O$) are in excellent agreement with those obtained from the formally exact method of NDIS [26], and gives confidence to the data analysis procedures that were employed.

Table 1
Data are given for the $g_{ZnO}(r)$s from the RMC simulations of the three aqueous zinc nitrate solutions and the $g_{NiO}(r)$ of the aqueous nickel nitrate solution

Solution	$T(K)$	r_0 (Å)	n_0	Δr (Å)
$Zn(NO_3)_2 \cdot 2H_2O$	30	2.05	2.7	0.20
($T_g = 201$ K)	160	2.08	2.9	0.23
	180	2.08	2.9	0.29
	195	2.09	3.3	0.41
$Zn(NO_3)_2 \cdot 6H_2O$	30	2.07	4.6	0.19
($T_g = 190$ K)	180	2.07	4.7	0.23
	185	2.09	4.7	0.23
$Zn(NO_3)_2 \cdot 12H_2O$	30	2.06	5.0	0.22
($T_g = 208$ K)	133	2.08	5.4	0.23
	162	2.08	5.3	0.23
	190	2.08	5.0	0.26
	202	2.07	5.7	0.28
	208	2.10	5.6	0.29
$Ni(NO_3)_2 \cdot 9H_2O$	30	2.07	6.1	0.18
($T_g = 200$ K)	155	2.07	6.2	0.19
	184	2.07	6.3	0.20
	195	2.07	6.4	0.28

Structural parameters are derived from a skewed Gaussian fit to the first feature in $g_{XO}(r)$. These values are: peak maximum, r_0, peak fwhm width, Δr, and hydration number n_0, calculated from the peak area.

We see that these data (Fig. 2 and Table 1), remain essentially unchanged during the heating process, and apart from the very high k region, are similar in form to that of a 1 m nickel nitrate solution (Fig. 2a). This suggests that although the free-energy model may well apply to the $Ni(NO_3)_2 \cdot 9H_2O$, it is highly unlikely that the configurational phase space extends to distances below the Ni-nearest neighbour distance. The result is therefore consistent with a relatively stable $[Ni(H_2O)_6]^{2+}$ unit as has been well established in numerous NDIS [26] and quasi-elastic neutron scattering studies [4,27]. We conclude that we can proceed to apply the same method of analysis to the Zn^{2+} ion.

Inspection of the DSC traces for the $Zn(NO_3)_2 \cdot 12H_2O$ (I) and $Zn(NO_3)_2 \cdot 2H_2O$(III). glasses (Fig. 1) shows them to have significantly higher T_gs than the $Zn(NO_3)_2 \cdot 6H_2O$ (II) sample. All of these glasses form crystals of $Zn(NO_3)_2 \cdot 6H_2O$, ice and $Zn(NO_3)_2$, with the $Zn(NO_3)_2 \cdot 6H_2O$ form being dominant (as far as composition allows). The main difference between samples I and III, is that the former shows a pre-feature at the start of the crystallisation process, whereas sample III shows only a smooth heat capacity change as it crystallises. It is noted that samples II and III could form a crystal with nearly the same stoichiometry. However, the $6H_2O$ sample has a lower glass transition point and a surprisingly large pre-crystallisation feature, which accounts for approximately 30% of the excess entropy.

The EXAFS data for $Zn(NO_3)_2 \cdot 12H_2O$ (Fig. 3a) shows a number of features. Most prominent is that at lowest temperature (30 K) the $\chi_{expt}(k)$ is significantly less sharp than the $\chi_{expt}(k)$s of the other two hydrated samples (Fig. 4a and Fig. 5a). Further, the feature centred at 3.7 $Å^{-1}$ seems to be composed of two peaks which swap their relative intensities as the sample is heated. This is consistent with small intermediate range structural modifications. The features in $k > 5$ $Å^{-1}$ have a small shift to higher k with increasing temperature, indicating a contraction in the local structural environment. The feature observed at 2 $Å^{-1}$ is almost identical to that seen in the low concentration experiments of Kuzmin et al. [15] and Munoz-Paez et al. [16]. From the invariance of the low k data with temperature, in particular one infers that the second hydration shell or hydrogen hydration sphere is less strongly perturbed that the first hydration sphere in the glass upon annealing.

The function $g_{ZnO}(r)$ shown in Fig. 3b represents the best RMC fit to the corresponding $\chi_{expt}(k)$. The data for these spectra are noisier than those obtained for the more concentrated solutions. This is probably due to the lower concentration of Zn^{2+} ions and a consequent lack of constraint in the RMC caused by the Zn–Zn ions being separated by a greater distance than the effective range of backscattered electron. The data for the sample I (Fig. 3b) show that during the annealing process the nearest neighbour distance shifts to higher value, and there is a corresponding increase in coordination number (Table 1). We conclude that two processes occur: firstly, the Zn^{2+} environment becomes progressively more relaxed by allowing other oxygen atoms to enter its immediate environment. Secondly, just prior to crystallisation this

environment becomes more disordered as illustrated by the broadening of the first peak in $g_{ZnO}(r)$.

The EXAFS spectra for $Zn(NO_3)_2 \cdot 6H_2O$ (Fig. 4a,b) at the two higher temperatures (180 K and 185 K) either side of the shoulder in the DSC trace (centred at 183 K) (Fig. 1). The structural change between 180 and 185 K is small, despite the large (30%) change in excess entropy as indicated in the DSC trace. Indeed, the only obvious differences in the EXAFS data are a loss of intensity at high k. This manifests itself as a large shoulder on the first peak of $g_{ZnO}(r)$. Similarities amongst data sets in the low k region shows that, in contrast to results for the $2H_2O$ and $12H_2O$ samples, there is no evidence for significant intermediate range structural change with temperature. The feature at 4.0 Å in the $g_{ZnO}(r)$, may arise from either a multiple scattering or a second coordination shell. Although it cannot be positively assigned, we prefer the latter explanation, as at these three sample concentrations a second coordination region would be expected.

The absence of a change in the short range order over the range 180–185 K implies that the large DSC feature in the $6H_2O$ sample is likely to have come about due to longer range interactions. We postulate therefore, that as the $6H_2O$ system is glassified, Zn^{2+} ions rapidly fill most of their nearest neighbour coordination shells with water molecules, leaving NO_3^- ions as peripheral to this shell. Thus, on approaching the glass transition, the system is able to undergo structural rearrangements which take place involving the $[Zn(H_2O)_6]^{2+}$ groups and it is this hydrogen bonded network that gives rise to the large excess entropy change in this system.

We observe that in the most concentrated glass discussed here ($Zn(NO_3)_2 \cdot 6H_2O$) the local order is significantly different from the crystalline state (Fig. 5a,b). The main differences observed in the $\chi_{expt}(k)$ spectra for each temperature are a splitting of the peak at 4 $Å^{-1}$. The comparison to the crystallised $Zn(NO_3)_2 \cdot 6H_2O$ spectrum (Fig. 4a) the glass spectrum has a higher fundamental frequency indicating a higher local density. Despite the large amount of change within $\chi_{expt}(k)$ the DSC trace is by far the simplest of the solutions with only the slightest hint of a pre-crystallisation feature between 180 and 190 K. However, in this glass, the first peak of $g_{ZnO}(r)$ to that of the $12H_2O$ glass is observed; the sharp frozen state relaxes to larger distances and then becomes strongly disordered immediately prior to crystallisation. This is probably due to the strong overlap and sharing of NO_3^- ions and H_2O molecules within the Zn^{2+} first coordination shell. On purely statistical grounds an oxygen atom of an NO_3^- anion must enter the first shell. In summary, the results for $Zn(NO_3)_2 \cdot 12H_2O$ where there is sufficient water to complete the hydration sphere show similar behaviour to those of the $Zn(NO_3)_2 \cdot 2H_2O$. We suggest that the origins of this behaviour is in the case of the former, due to the hydration of the Zn^{2+} being insufficiently strong (cf. Ni^{2+}) to avoid interaction with NO_3^- ions and water molecules of the second hydration sphere. This situation is particularly the case for NO_3^- ions, which are planar and can displace water. For the case of the $Zn(NO_3)_2 \cdot 2H_2O$ system, the Zn^{2+} coordination is mixed with incomplete hydration. Although there is no requirement for water molecules to be displaced to allow NO_3^- penetration into the Zn^{2+} hydration sphere, when NO_3^- enters this region, significant loss of hydration binding and order are clearly observed.

Therefore, for zinc nitrate solutions with water fractions above $6H_2O$ there is an orientational bonding in the second hydration sphere the nature of which underpins the glassy properties of the system. For solutions with water fractions below $6H_2O$ the coordination is likely to be ionic due to incomplete Zn^{2+} hydration. We also find that the NO_3^- ion is unable to act as an effective oxygen donor to the hydration sphere of Zn^{2+}, at higher temperatures, probably due to its rotation. This result may explain why solution hydrates of nitrate salts are easier to glassify than those of chloride salts.

The results above also explain how Zn^{2+} plays an important role in biological processes. Indeed the results of the glassification study presented above link in with those from neutron quasi-elastic scattering and molecular dynamics simulation studies of Cu,Zn superoxide dismutase [28,29] which indicate that a glasslike transition appears approximately 200 K, i.e. in exactly the same regime

found in the current work. We also note the result for Zn^{2+} stands in marked contrast to that for Ni^{2+}, which has a well-defined six-fold coordination in solution and appears to have no biological role whatsoever!

4. Conclusions

The results presented above show that EXAFS, when combined with state-of-the-art RMC simulations, may be used to provide useful structural information on complex liquids and glasses. By exploiting the fact that the scattering process is centred on the back-scattered electron, it is possible to investigate the annealing process in the region of the glass transition in terms of the degree of disorder around the photoabsorbing ion. We conclude that the pre-crystallisation features in the DSC results are linked to the formation of second hydration shell structures. This process arises at the expense of the ordering within the Zn^{2+} first coordination shell, which unsurprisingly becomes less ordered with increasing temperature. In the case of a $Zn(NO_3)_2 \cdot 2H_2O$ solution, there is insufficient water to support the hydrogen-bonding network and to stabilise a directionally bonded second coordination sphere, i.e. a configuration that requires co-operative motion. Instead, the system behaves like a simple molten salt with electrostatic interactions. This interpretation of the three hydrated salt solutions also helps in explaining the seemingly random order for the glass transition temperatures. The $Zn(NO_3)_2 \cdot 12H_2O$ has more water than that of the crystal but insufficient to allow an ice-like hydrogen bond structure to be formed quickly. Consequently, large structural rearrangements are needed on crystallisation to remove the water from the crystallising regions. The $Zn(NO_3)_2 \cdot 6H_2O$ sample has no excess water and is able to adopt rapidly the crystalline structure through progressive rearrangements. Thus, the ionic length scale is important in the cooling process. The improvements described above for the analysis of EXAFS data for disordered systems will enable more far reaching studies of structural and dynamical processes to be carried out. For example, because EXAFS is sensitive at low concentrations of the absorbing species, results for the local structure of transition metal ions such as Zn^{2+}, Fe^{2+}, Fe^{2+} and Cu^{2+} in bio-molecular materials can be obtained in regimes of normal biological activity.

Acknowledgments

The authors would like to thank Adriano Filliponi and Andrea Di Cicco for their helpful comments on data analysis procedures, and the provision of the GNXAS source code. We also thank M. Borowski, G. Subias and R. Weigel at BM29, ESRF for their assistance in carrying out the experiments.

References

[1] W. Kauzmann, Nature of the glassy state, Chem. Rev. 43 (1948) 219.
[2] P. Mason, G. Neilson, C. Dempsey, A. Barnes, J. Cruickshank, The hydration structure of guanidinium and thiocyanate ions; implications for protein stability in aqueous solution, submitted.
[3] R. Bohmer, Phase tranistion kenetics, J. Non-Crys. Solids 172–174 (1994) 628.
[4] N. Hewish, J. Enderby, W. Howells, The dynamics of water molecules in ionic solution, Solid State Phys. 16 (1983) 1777.
[5] M. Wilson, P. Madden, 'Prepeaks' and 'first sharp diffraction peaks' in computer simulations of strong and fragile ionic liquids, Phys. Rev. Lett. 72 (1994) 3033.
[6] C.A. Angell, E. Sare, Glass-forming composition regions and glass transition temperatures for aqueous electrolyte solutions, J. Chem. Phys. 52 (1970) 1058.
[7] A. Barrat, R. Burioni, M. Mezard, Dynamics within metastable states in a mean-field spin glass, J. Phys. A 29 (1996) L81.
[8] W. Kauzmann, Dielectric relaxation as a chemical rate process, Rev. Mod. Phys. 14 (1942) 12.
[9] R. Schilling, Mode-coupling theory for translational and orientational dynamics near the ideal glass transition, J. Phys. C: Condens. Mat. 12 (2000) 6311.
[10] J.C. Schön, Preferential trapping on energy landscapes in regions containing deep-lying minima: the reason for the success of simulated annealing?, J. Phys. A: Math. Gen. 30 (1997) 2367.
[11] S. Ansell, G.W. Neilson, Structure of aqueous ammonium calcium nitrate glass former studied by neutron diffraction, J. Phys. C: Condens. Mat. 11 (1999) 7035.
[12] D. Kivelson, W. Steffen, G. Meier, A. Patkowski, A possible molecular structural indicator of the liquid–glass transition, J. Chem. Phys. 95 (1991) 1943.

[13] G. Neilson, A. Adya, S. Ansell, Review of complex liquids, Annu. Rep. Roy. Soc. Chem. Sect. C 98 (2002) 273.
[14] A. Fillipponi, EXAFS for liquids, J. Phys. C: Condens. Mat. 13 (2001) R23.
[15] A. Kuzmin, S. Obst, J. Purans, X-Ray absorption spectroscopy and molecular dynamics studies of Zn^{2+} hydration in aqueous solution, J. Phys. C: Condens. Mat. 9 (1997) 10065.
[16] A. Munoz-Paez, R.R. Pappalardo, E.S. Marcos, Determination of the second hydration shell of Cr^{3+} and Zn^{2+} in aqueous solution by extended X-ray absorption fine structure, J. Am. Chem. Soc. 117 (1995) 11 710.
[17] R. Caminiti, P. Cucca, M. Monduzzi, G. Saba, G. Criponi, Divalent metal-acetate complexes in concentrated aqueous solutions. An X-ray diffraction and NMR spectroscopy study, J. Chem. Phys. 81 (1984) 543.
[18] P. dÁngelo, A.D. Nola, A. Fillipponi, N. Pavel, D. Roccatano, An extended X-ray absorption fine structure study of aqueous solutions by employing molecular dynamic simulations, J. Chem. Phys. 100 (1994) 985.
[19] A. Fillipponi, M. Borowski, D.T. Bowron, S. Ansell, A.D. Cicco, S.D. Panfilis, et al., An experimental station for advanced research on condensed matter under extreme conditions at the European Synchrotron Radiation Facility-BM29 beamline, Rev. Sci. Inst. 71 (2000) 2422.
[20] J.M. de Leon, Y. Yacoby, E. Stern, J. Rehr, A flexible method for fitting EXAFS spectra: application to structural phase transitions, Physica B 158 (1989) 263.
[21] J. Rehr, J.M. de Leon, S. Zabinskiy, R. Albers, Theoretical X-ray absorption and structure standards, J. Am. Chem. Soc. 113 (1991) 5135.
[22] A. Filliponi, A.D. Cicco, GNXAS: A software package for advanced EXAFS multiplescattering calculations and data-analysis, Task Quarterly 4 (2001) 1.
[23] N. Binstead, S. Gurman, J. Campbell, P. Stephenson, EXCURVE, Tech. rep., Daresbury Lab. Project (1982).
[24] R.L. McGreevy, L. Pusztai, The structure of molten salts, Mol. Simulat. 1 (1988) 359.
[25] Y. Babanov, V. Vasin, A. Ageev, N. Eishov, A new interpretation of EXAFS spectra in real space. I. General formalism, Phys. Status Solidi B 105 (1981) 747.
[26] I. Howell, G. Neilson, Ni^{2+} coordination in concentrated aqueous solutions, J. Mol. Liq. 73–74 (1997) 337.
[27] P. Salmon, M.-C. Bellissent-Funel, G. Herdman, The dynamics of aqueous Zn^{2+} solutions: a study of incoherent quasi-elastic neutron scattering, J. Phys C: Condens. Mat. 2 (1990) 4297.
[28] C. Andreani, A. Filabozzi, F. Menzinger, A. Desideri, A. Deriu, D.D. Cola, Dynamics of hydrogen atoms in superoxide desmutase by quasielastic neutron scattering, Biophys. J. 68 (1995) 2519.
[29] S. Melchionna, M. Falconi, A. Desideri, Effect of temperature and hydration on protein fluctuations: molecular dynamics simulation of Cu, Zn superoxide dismutase at six different temperatures. Comparison with neutron scattering data, J. Chem. Phys. 108 (1998) 6033.